Contents lists available at ScienceDirect

Transactions of Nonferrous Metals Society of China

36(2026) 218−230

www.tnmsc.cn

# Composite descriptor for screening mechanical properties in high-entropy diborides

Yong FAN [a], Jin-feng NIE [a,*], Jin WANG [a], Zhi-gang DING [a], Wei LIU [a,b,**], Yong-hao ZHAO [a,c]

[a] Nano and Heterogeneous Materials Center, School of Materials Science and Engineering, Nanjing University of Science and Technology, Nanjing 210094, China;

[b] State Key Laboratory of Rare Earth Resource Utilization, Changchun Institute of Applied Chemistry, Chinese Academy of Sciences, Changchun 130022, China;

[c] School of Materials Science and Engineering, Hohai University, Changzhou 213022, China

**Abstract:** The composition−property relationship of 18 quaternary high entropy diborides (HEBs) consisting of boron and IVB, VB and VIB transition metals (TM) was investigated using first-principles calculations. A valence electron concentration−relative electronegativity (VEC−REN) composite descriptor was developed to effectively predict the mechanical properties of HEBs. The results demonstrate that with a fixed VEC, the rise of the REN makes HEBs harder but more brittle when the electronegativity of doped TM atoms is lower than that of boron atoms. However, HEBs become softer and more ductile as REN increases if the doped TM atoms have higher electronegativity than boron atoms. The VEC−REN composite descriptor can accurately classify and predict the mechanical properties of HEBs with different components, which provides important theoretical guidance for the rapid design and development of novel high-entropy ceramic materials.

**Keywords:** first-principles; high-entropy diborides; valence electron concentration; relative electronegativity; mechanical properties

## 1 Introduction

Since 2004, high entropy alloys (HEA) have attracted significant attention due to the excellent performance under extreme environments, including high temperature, irradiation and nuclear reactors [1−5]. HEAs, composed of five or more primary elements in atomic percentages ranging from 5% to 35%, offer a broad compositional space for tailoring material properties. With an increasing demand for higher performance, the design and exploration of new materials with desirable properties have become critical areas of research [6,7]. Recently, the high-entropy design concept has been introduced to ceramic systems, including oxides, borides, carbides, and nitrides [8−14].

Among the high-entropy ceramic (HEC) materials, high entropy transition metal diborides (HEBs) have emerged as promising ultra-high temperature ceramics (UHTCs) due to their exceptional hardness, high-temperature stability, and oxidation resistance [15−17]. The excellent performance of HEBs makes them have great application potential in extreme environments, such as hypersonic vehicles, ultra-high temperature thermal barrier coatings and nuclear reactors. The wide composition space of HEC provides the

**Corresponding author:** *Jin-feng NIE, Tel: +86-25-84303281, E-mail: niejinfeng@njust.edu.cn;
**Wei LIU, Tel: +86-431-85262487, E-mail: weiliu@ciac.ac.cn

https://doi.org/10.1016/S1003-6326(25)66959-7

Received 3 April 2024; accepted 11 December 2024

possibility for designing the desired mechanical properties of materials, but the research on HEBs is still in its early stages. Currently, the research is focused on improving the mechanical properties by compositional optimization and advanced synthesis techniques based on experiments [18,19].

A major challenge is the fact that HEBs commonly exhibit extreme brittleness in addition to their high hardness, thereby significantly limiting their practical applications. This is due to the fact that the prepared HEBs are mainly composed of IVB and VB refractory transition metal diborides ($TMB_2$s), such as $ZrB_2$ and $TiB_2$, which are known for their limited ductility [20]. As for VIB transition metal diborides, like $CrB_2$, $MoB_2$ and $WB_2$, although predicted to be ductile UHTCs, they have relatively low hardness and are thermodynamically unstable. Only a few studies have reported HEBs containing more than two VIB group elements due to their low hardness and thermodynamic instability [21,22].

Besides, the fundamental understanding of the relationship linking the appropriate properties of a HEC phase to its intrinsic corresponding components remains the biggest challenge in this field. To classify and predict properties of HEBs, an accurate and appropriate descriptor for HEBs is urgently needed. Addressing this need, some attempts have been reported to explore the phase formation and mechanical properties of HECs using the density functional theory (DFT) based on first-principles calculations [23−25]. For instance, GUO and LIU [26] claimed that the mixing enthalpy ($\Delta H_{mix}$), electronegativity difference ($\Delta\chi$) and valence electron concentration (VEC) are crucial for the formation of the single phase solid solution of HEA. LIU et al [27] constructed a new thermodynamic parameter ($\Omega$) along with the structural parameter atomic size difference ($\delta$) and established the $\Omega$−$\delta$ criterion to predict the formation ability of fifteen quaternary HEBs.

Further investigation is required to study the relationship between the descriptors of formation ability and the mechanical properties of the HEBs. GU et al [28] conducted extensive research on binary metal diborides and claimed that relative electronegativity (REN) plays a key role in determining property trends by capturing relative charge redistribution. Although the composite VEC-REN descriptor was proposed to accurately sort mechanical properties of binary metal diborides, the space for modulation of material design is finite compared to high entropy systems.

In this work, the phase stability and mechanical properties of 18 quaternary transition metal diborides using first-principles calculations were systematically investigated. This work is expected to accelerate the discovery and design of HEC materials possessing appropriate and adjustable properties, offering new pathways for applications in extreme environments.

## 2 Computational methods

The structure of the $AlB_2$-type high-entropy metal diborides consists of a cationic sublattice and an anionic sublattice respectively occupied by transition metal (TM) atoms with equal atomic ratios and the boron atoms, as shown in Fig. 1(a). The special quasi-random structure technique was

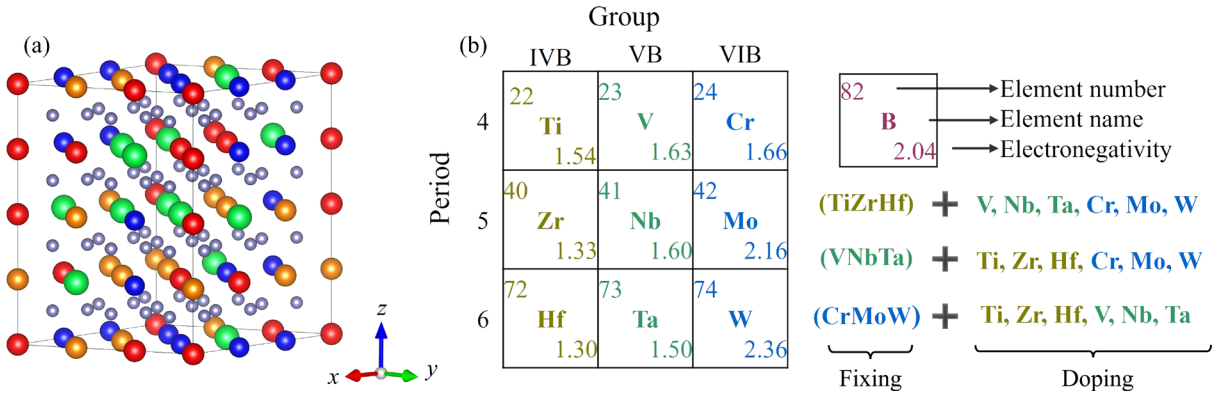


**Fig. 1** (a) Crystal structure of high entropy diborides (The grey spheres represent boron atoms, and other colored spheres represent transition metals (Ti, Zr, Hf, V, Nb, Ta, Cr, Mo and W)); (b) Doped schemes of 18 quaternary high-entropy diborides

employed to generate disordered high entropy solid solution using the Alloy Theoretic Automated Toolkit (ATAT) [29,30]. The bulk supercell (3×3×4) with 108 atoms was selected for the calculations. The first-principles calculations were conducted using Vienna ab initio simulation package (VASP) code with the project-augmented wave method and the Perdew−Burke−Ernzerhof version of the exchange correlation functional [31,32]. The VASP calculations were performed using the Gamma $k$-point mesh of 4×4×3, with the cutoff energy of the plane wave basis set to be 400 eV. The convergence criteria during the optimization were set to be $1\times10^{-4}$ eV and 0.02 eV/Å for the electronic relaxation process and the ionic relaxation loop, respectively.

Figure 1(b) shows the design principle and electronegativity values of all the atoms involved, according to the Pauling scale [33]. The REN values for group-IVB transition metal atoms show a noticeable decline from Ti to Zr and then to Hf. The value of the group-VB TM atoms exhibits a similar trend, ranging from V to Nb and finally to Ta, whereas the values of group-VIB TM atoms show a completely opposite pattern, from Cr (1.66) to Mo (2.16) and ultimately to W (2.36). In order to find the appropriate properties of HEBs, we designed 18 high-entropy diborides by using a fixed-doped-TM structure with TM atoms from groups IVB, VB, and VIB. In particular, three TM atoms are taken from one group, denoted as fixed atoms, while the fourth TM atom is chosen from another different group as the doped atom in each quaternary HEB model. By adjusting the doped atoms from group IVB to VIB TM atoms, the REN values of the quaternary HEBs can be effectively tuned while hosting the same VEC.

The elastic constants were acquired by strain−stress relations to investigate the mechanical properties of the 18 quaternary HEBs. Then, the bulk modulus $B$, shear modulus $G$, Young's modulus $E$ were derived from the calculated elastic stiffness constants by Voigt–Reuss–Hill (VRH) approximation [34]. The values of $G/B$ and Poisson's ratio ($v$) were utilized to evaluate the ductility of the HEBs. The formula for Poisson's ratio is $v=(3B-2G)/(6B+2G)$. A material exhibits brittleness properties if $G/B>0.57$ or $v<0.26$ [35,36]; The hardness can be calculated by the formulation: $H=0.92(G/B)^{1.37}G^{0.708}$ [37].

# 3 Results

## 3.1 Crystal structure and thermodynamic stability

In order to assess the validity of the formation of 18 quaternary high-entropy diborides, their geometry optimized lattice parameters are first calculated and the results are listed in Table 1. The calculated lattice constants ($a$ and $c$) of VNbTaTiB8, VNbTaZrB8 and VNbTaHfB8 are similar to the results in the previous study [27]. The calculated values of TiZrHfTaB8, TiZrHfCrB8 and TiZrHfVB8

**Table 1** Lattice parameters and $c/a$ ratio for studied 18 quaternary high-entropy diborides

| Material | VEC | Source | Lattice constant/Å | | $c/a$ |
|---|---|---|---|---|---|
| | | | $a$ | $c$ | |
| TiZrHfVB8 | 10.25 | This work | 3.087 | 3.345 | 1.083 |
| | | Exp. [38] | 3.12 | 3.41 | 1.092 |
| TiZrHfNbB8 | 10.25 | This work | 3.114 | 3.401 | 1.092 |
| TiZrHfTaB8 | 10.25 | This work | 3.112 | 3.398 | 1.092 |
| | | Exp. [39] | 3.105 | 3.338 | 1.091 |
| TiZrHfCrB8 | 10.5 | This work | 3.078 | 3.343 | 1.086 |
| | | Exp. [40] | 3.109 | 3.387 | 1.089 |
| TiZrHfMoB8 | 10.5 | This work | 3.101 | 3.374 | 1.088 |
| TiZrHfWB8 | 10.5 | This work | 3.102 | 3.376 | 1.088 |
| VNbTaTiB8 | 10.75 | This work | 3.065 | 3.226 | 1.053 |
| | | Exp. [27] | 3.04 | 3.20 | |
| VNbTaZrB8 | 10.75 | This work | 3.095 | 3.315 | 1.071 |
| | | Exp. [27] | 3.08 | 3.27 | |
| VNbTaHfB8 | 10.75 | This work | 3.089 | 3.303 | 1.069 |
| | | Exp. [27] | 3.06 | 3.23 | |
| VNbTaCrB8 | 11.25 | This work | 3.046 | 3.184 | 1.045 |
| VNbTaMoB8 | 11.25 | This work | 3.067 | 3.247 | 1.059 |
| VNbTaWB8 | 11.25 | This work | 3.069 | 3.249 | 1.059 |
| CrMoWTiB8 | 11.5 | This work | 3.03 | 3.187 | 1.052 |
| CrMoWZrB8 | 11.5 | This work | 3.058 | 3.299 | 1.079 |
| CrMoWHfB8 | 11.5 | This work | 3.049 | 3.299 | 1.082 |
| CrMoWVB8 | 11.75 | This work | 3.031 | 3.143 | 1.037 |
| CrMoWNbB8 | 11.75 | This work | 3.054 | 3.245 | 1.063 |
| CrMoWTaB8 | 11.75 | This work | 3.049 | 3.245 | 1.064 |

also agree well with the experimental results [38−40]. Both of these results demonstrate the dependability of the current calculations.

The difference of lattice constant ($\delta_a$ and $\delta_c$) is an empirical index for predicting the formation of HEBs. The critical lattice size difference to form a single-phase HEA structure is 6.6%. The lattice constant difference for $AlB_2$-type HEB can be expressed as [27]

$$\delta_a = \sqrt{\sum_{i=1}^{N} x_i \left(1 - a_i / \overline{a}\right)^2}, \quad \overline{a} = \sum_{i=1}^{N} x_i a_i \tag{1}$$

$$\delta_c = \sqrt{\sum_{i=1}^{N} x_i \left(1 - c_i / \overline{c}\right)^2}, \quad \overline{c} = \sum_{i=1}^{N} x_i c_i \tag{2}$$

where $x_i$ is the atomic fraction of the $i$-th element; $a_i$ and $c_i$ are the lattice constants of their corresponding single-component metal diborides, respectively; $\overline{a}$ and $\overline{c}$ are the average lattice constants of different diboride ceramics; $N$ is the number of metal elements in the ceramic.

Subsequently, the calculated $\delta_a$ and $\delta_c$ of the HEBs are given in Figs. 2(a, b), respectively. The computed $\delta_a$ values are smaller than $\delta_c$ because of the different electronic structure and chemical bonding nature of the various planes of HEBs. ZHOU et al [20] provided a detailed chemical bonding analysis of transition metal diboride. They confirmed that the TM—TM bonding is metallic, evidenced by a triangular accumulation of electrons between neighboring TM atoms. The B—B bonding is covalent, with strong electron localization indicating $\sigma$-type covalent bonds formed by overlapping hybridized B $sp^2$ orbitals, and $\pi$-type covalent bonds formed through the overlapping of B $p_z$ orbitals. The TM-B bonding is primarily ionic due to charge transfer from TM to B, but there is also evidence of covalent bonding from the interaction between TM-d and B-p orbitals. WANG et al [25] investigated the bonding feature for $(Hf_{0.2}Zr_{0.2}Ta_{0.2}M_{0.2}Ti_{0.2})B_2$, showing similar bonding characteristics to the $TMB_2$. The chemical bonding on the boron plane is covalent, while on the metal plane, it is metallic. The bonding between metal and boron exhibits mixed ionic-covalent characteristic. The M—B or M—M bonds accommodate the internal strain in the structure, rather than by distorting the 2D rigid boron net resulting in $\delta_a$ values smaller than $\delta_c$. Among the 18 quaternary HEBs, except for TiZrHfCrB8 and CrMoWZrB8,

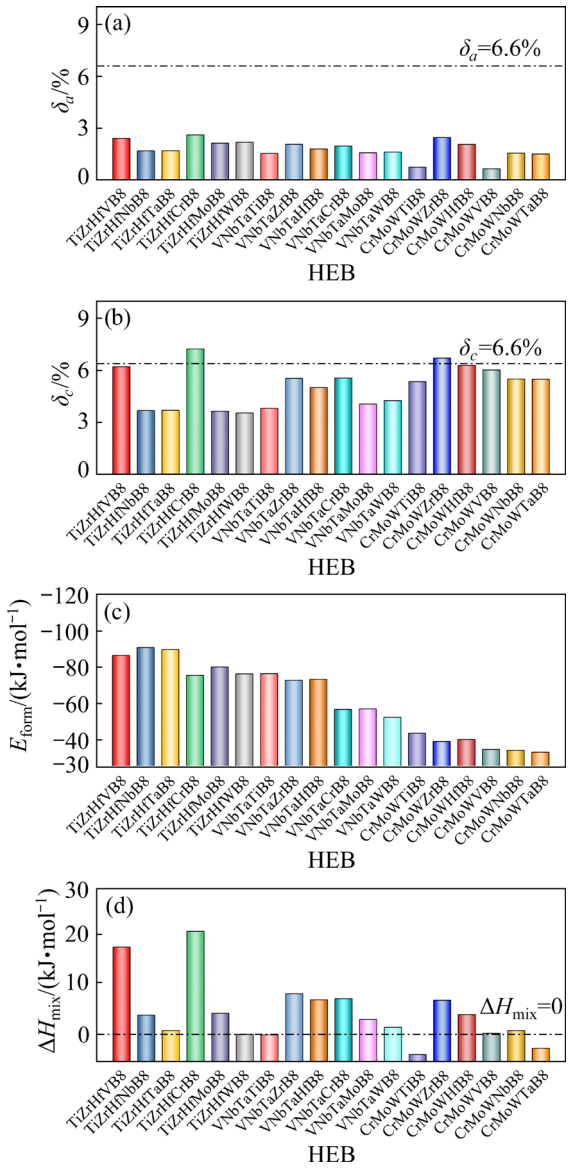


**Fig. 2** (a) Calculated lattice constant $a$ difference ($\delta_a$), (b) calculated lattice constant $c$ difference ($\delta_c$), (c) formation energy ($E_{form}$), and (d) mixing enthalpy ($\Delta H_{mix}$) of 18 high-entropy metal diborides

the $\delta_a$ and $\delta_c$ are below 6.6%, indicating that they can form a single-phase HEB structure. The large $\delta_a$ and $\delta_c$ may result in a large energy of lattice distortion in TiZrHfCrB8 and CrMoWZrB8, in particular TiZrHfCrB8. However, the formation energy ($E_{form}$) for TiZrHfCrB8, close to that for TiZrHfNbB8, suggests that a stable structure can be achieved by high configurational entropy, potentially overcoming the enthalpy disadvantage. This is also supported by the experimental results, which pointed out the importance of thermal annealing for cation diffusion, resulting in chemical homogenization to obtain the configurational

entropy required for stable high-entropy ceramics [38]. Thus, it can be concluded that TiZrHfCrB8 and CrMoWZrB8 with large $\delta$ can form the stable high-entropy structure.

Besides the lattice constant difference, the chemical stability of the 18 HEBs could be assessed by the formation energy [41]:

$$E_{\text{form}}=\left(E_{\text{tot}}-\sum N_i E_{i\text{-bulk}}\right)/\sum N_i \quad (3)$$

where $E_{\text{tot}}$ is the total energy of the HEBs, $E_{i\text{-bulk}}$ is the energy of one atom, and $N_i$ is the number of atoms in the HEBs. In general, a relatively negative $E_{\text{form}}$ is associated with high chemical stability.

As depicted in Fig. 2(c), the $E_{\text{form}}$ of all four-metal diborides is negative, indicating that the HCP-structured HEBs are thermodynamically stable. This is caused by the high entropy effect of multiple components, which in turn promotes the formation of simple solid solution structures.

The thermodynamic stability of HEBs can be analyzed by the Gibbs free energy change of mixing ($\Delta G_{\text{mix}}$), which can be expressed as [42]

$$\Delta G_{\text{mix}}=\Delta H_{\text{mix}}-T\Delta S_{\text{mix}} \quad (4)$$

where $T$ is the thermodynamic temperature, $\Delta H_{\text{mix}}$ is the mixing enthalpy and $\Delta S_{\text{mix}}$ is the mixing entropy.

The $\Delta H_{\text{mix}}$ for HEB system can be obtain by

$$\Delta H_{\text{mix}}=\left(E_{\text{tot}}-\sum N_i E_i^{\text{MeB}_2}\right)/\sum N_i \quad (5)$$

where $E_i^{\text{MeB}_2}$ is the energy of the individual metal diboride.

Figure 2(d) shows the mixing enthalpies of 18 HEBs. All of the mixing enthalpies, except for those of CrMoWTiB8 and CrMoWTaB8, are positive. This indicates that the formation of HEBs is an endothermic process. Nevertheless, all the mixing enthalpies are relatively small, with the maximum value being merely 20 kJ/mol.

The $\Delta S_{\text{mix}}$ of an $N$-element solution can be evaluated by [43]

$$\Delta S_{\text{mix}}=-\frac{R}{3}\sum_{i=1}^{N} x_i \ln x_i \quad (6)$$

where $R$ is the molar gas constant.

The calculated $\Delta S_{\text{mix}}$ values of the quaternary HEBs were 0.46$R$. The formation of a stable high-entropy diboride is determined by the combined effect of mixing enthalpy and entropy. At an elevated temperature, the effect of mixing entropy dominates over that of the mixing enthalpy, resulting in a negative Gibbs free energy of mixing, and a stable HEB solid solution structure can be formed. The multicomponent metal diborides are driven by negative $\Delta G_{\text{mix}}$ to form stable single-phase HEB.

### 3.2 Elastic constants of HEBs with changing VEC

The mechanical stability of the HEBs based on the results of elastic constants is studied. The obtained five independent elastic constants of HEBs are listed in Table 2. The elastic stability criteria for hexagonal structure can be judged from the Born−Huang criterion [44]. The criteria are completely satisfied, demonstrating that all the HEBs are mechanically stable. The $C_{44}$ values calculated for the 18 HEBs examined in this study are depicted in Fig. 3, which take into account the shear behaviors along $[10\bar{2}0]$ directions for the hexagonal symmetry structure. At each VEC, the data are widely dispersed but show a distinct overall decreasing pattern, starting from an average of 246 GPa at VEC=10.25 and decreasing to 97 GPa at

**Table 2** Calculated elastic constants ($C_{ij}$) of 18 HEBs (GPa)

| Material | $C_{11}$ | $C_{12}$ | $C_{13}$ | $C_{33}$ | $C_{44}$ |
|---|---|---|---|---|---|
| TiZrHfVB8 | 599 | 79 | 127 | 425 | 240 |
| TiZrHfNbB8 | 578 | 85 | 146 | 418 | 248 |
| TiZrHfTaB8 | 579 | 92 | 150 | 420 | 249 |
| TiZrHfCrB8 | 588 | 83 | 132 | 407 | 217 |
| TiZrHfMoB8 | 597 | 83 | 145 | 425 | 233 |
| TiZrHfWB8 | 592 | 85 | 159 | 407 | 220 |
| VNbTaTiB8 | 638 | 108 | 150 | 464 | 238 |
| VNbTaZrB8 | 602 | 103 | 164 | 433 | 228 |
| VNbTaHfB8 | 610 | 104 | 169 | 432 | 228 |
| VNbTaCrB8 | 616 | 132 | 172 | 429 | 170 |
| VNbTaMoB8 | 601 | 134 | 190 | 427 | 183 |
| VNbTaWB8 | 602 | 137 | 195 | 427 | 182 |
| CrMoWTiB8 | 601 | 128 | 183 | 386 | 143 |
| CrMoWZrB8 | 525 | 135 | 197 | 344 | 113 |
| CrMoWHfB8 | 565 | 121 | 188 | 347 | 114 |
| CrMoWVB8 | 584 | 140 | 196 | 370 | 98 |
| CrMoWNbB8 | 556 | 130 | 182 | 405 | 95 |
| CrMoWTaB8 | 512 | 203 | 204 | 355 | 98 |

VEC=11.75. This suggests that the shear deformation resistance of HEBs tends to decrease as the VEC increases. Furthermore, there is considerable overlap in the ranges of $C_{44}$ for different VEC values. For example, the $C_{44}$ values have ranges of 240−249 GPa at VEC=10.25, 217−233 GPa at VEC=10.5 and 228−238 GPa at VEC=10.75. The phenomenon of the expanded property range shows that VEC parameter alone is insufficient to accurately classify and predict the mechanical characteristics of HEBs. Therefore, a new descriptor is needed for rational material design.

Figure 4 displays the results of the elastic parameters, $C_{11}$ and $C_{33}$, of the examined HEBs. These elastic parameters can be defined as the bonding strength along [10$\bar{1}$0] and [0001] directions under the tensile stress. In contrast to $C_{44}$, the calculated values of $C_{11}$ and $C_{33}$ exhibit significant scatter even at the same VEC. Moreover,

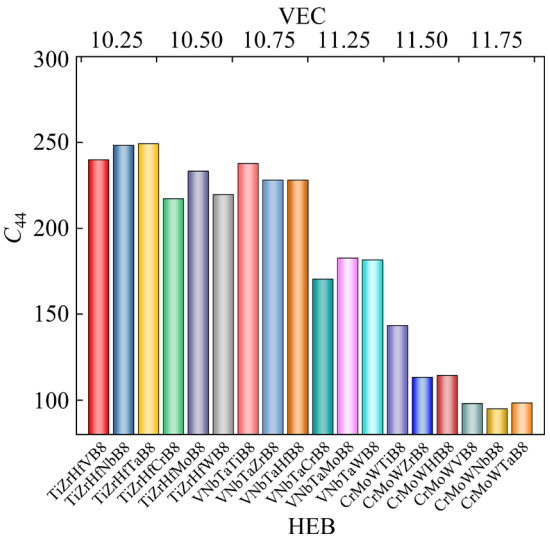


**Fig. 3** Calculated elastic parameters $C_{44}$ values as function of VEC of 18 high-entropy metal diborides

the $C_{11}$ values are evidently greater than the $C_{33}$ values, suggesting the anisotropy of compressional characteristics along different directions of the HEBs.

Therefore, the calculation was performed to determine the compressive anisotropy ratio ($C_{33}/C_{11}$), which is closely related to anisotropic deformation. For a completely isotropic system, the compressional anisotropy ratio is close to 1.0 [45]. Figure 5(a) shows the $C_{33}/C_{11}$ values of the HEB investigated. It can be seen that $C_{33}/C_{11}$ values remain well in a range below 1.0, indicating the significant anisotropy of the elastic parameters for the HEBs. Besides, this parameter is also extremely dispersed, demonstrating that VEC is not appropriate indicator to capture anisotropic behaviors. Another method of assessing the mechanical property anisotropy is examining the relationship of $G/B$ with $v$. A material is isotropic when the slope is approximately −2.6 within the $v$ range of 0.2−0.45 [46]. The linear curve is shown in Fig. 5(b) and the regions of brittleness and ductility are separated by $G/B$=0.57 and $v$=0.26. The slope of the $G/B$ curve is −3.17, indicating that the mechanical properties of the HEBs are significantly anisotropic.

The effect of varying VEC on $B$, $G$, $G/B$ and $v$ for the 18 quaternary high-entropy diborides studied here is examined, and the calculated results are illustrated in Fig. 6. The variation trend of these mechanical properties is similar and the scattering range of all parameters is very large. The $B$ represents the ability of a material to resist volume change under pressure, while the $G$ represents the material's ability to sustain shape deformation [47]. When the VEC increases, the values of $B$ also

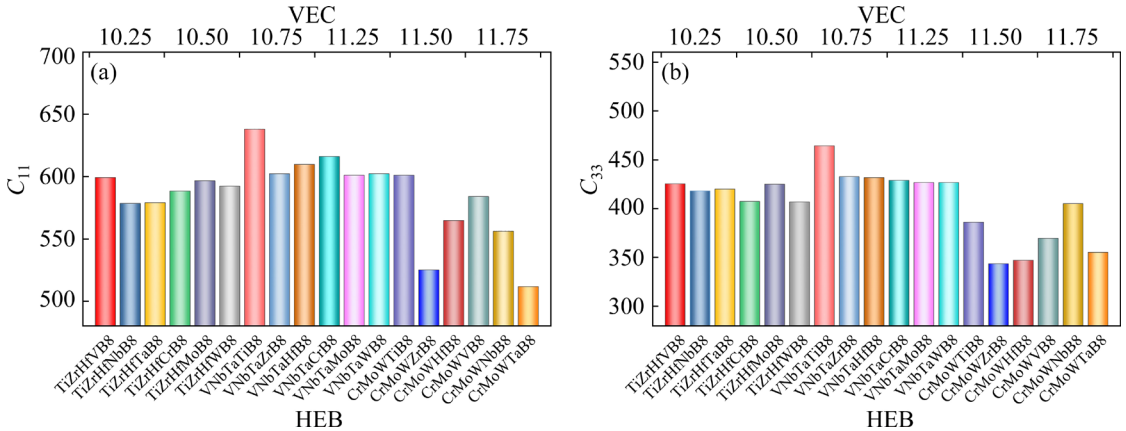


**Fig. 4** (a) Elastic parameters $C_{11}$ and (b) elastic parameters $C_{33}$ of all HEBs versus VEC changing from 10.25 to 11.75

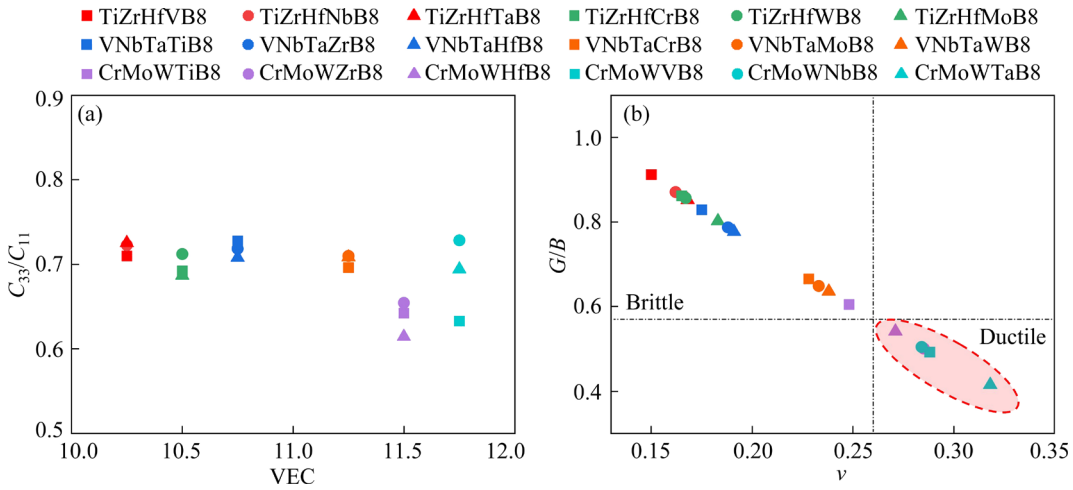


**Fig. 5** (a) Calculated results of $C_{33}/C_{11}$ for all diborides versus VEC (10.25−11.75); (b) Linear relation between $G/B$ and $\nu$

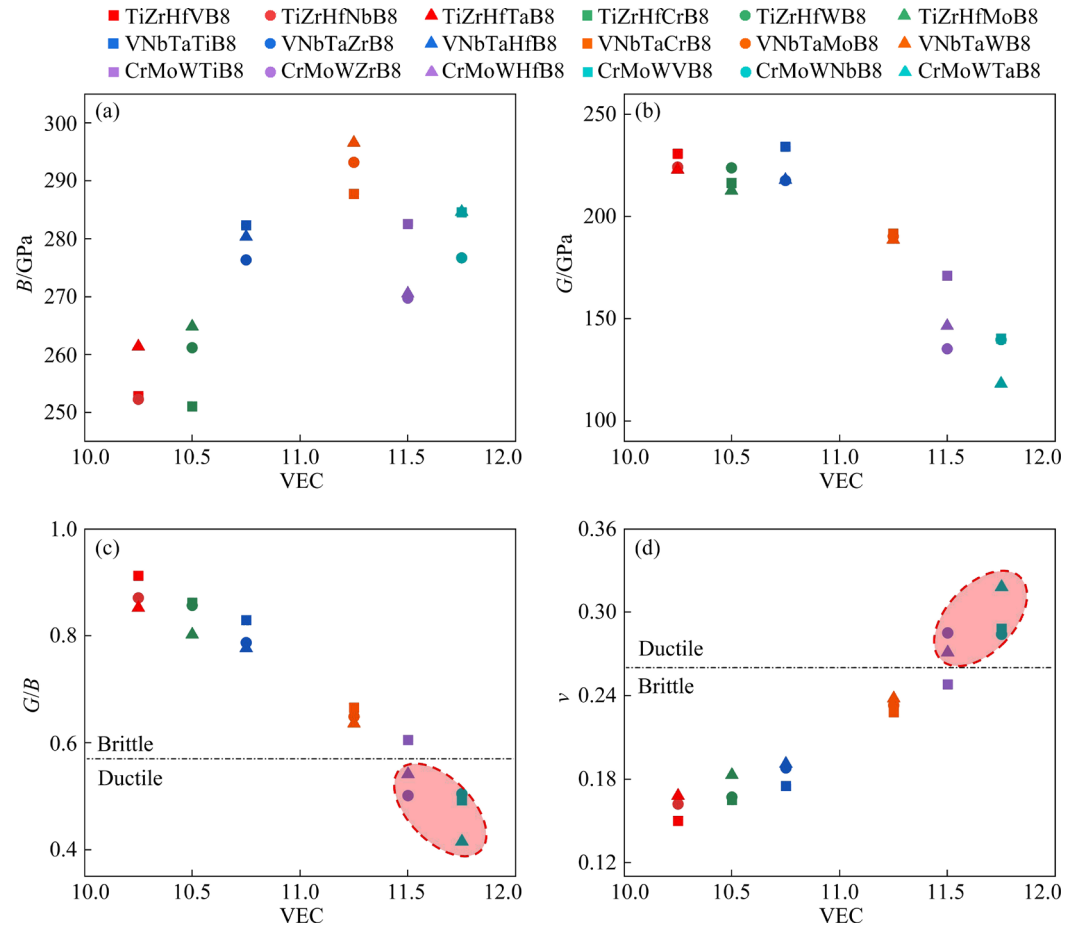


**Fig. 6** (a) Bulk modulus ($B$) for 18 high-entropy metal diboride with VEC increasing from 10.25 to 11.75; (b) Shear modulus ($G$) for 18 high-entropy metal diboride with VEC increasing from 10.25 to 11.75; (c) Variation trends of $G/B$ with VEC; (d) Variation trends of Poisson's ratio ($\nu$) with VEC

increase (Fig. 6(a)), whereas the $G$ values Fig. 6(b) exhibit an opposite trend compared to the $B$. These $B$ and $G$ values exhibit a spread of approximately 20−30 GPa for every fixed VEC. As VEC increases, the $G/B$ values (Fig. 6(c)) display a downward trend, while $\nu$ values (Fig. 6(d)) increase. Here, a significant number of ductile systems are observed, including CrMoWZrB8, CrMoWHfB8, CrMoWVB8, CrMoWNbB8, CrMoWTaB8. The VEC value that is crucial for the transition from brittle to ductile is

11.5. Although the overall trend of the mechanical properties of HEB with the VEC is comparable to the reported one of binary metal diborides, the mechanical properties of HEB have a very large scattering range at the same total VEC [48]. A typical example is the compounds, CrMoWHfB8 and CrMoWTiB8, which have the same VEC of 11.5 but show different mechanical properties. Based on the values of $G/B$ and $\nu$, it can be concluded that the former is ductile, while the latter is brittle.

Figures 7(a, b) plot the dependence of the hardness and Young's modulus on the VEC of the HEBs, respectively. $H$ represents a material's intrinsic resistance to deformation when a force is applied [49], while $E$ indicates a material's resistance to tensile or compressive deformation. As VEC increases, $H$ decreases from an average of approximately 37.5 GPa at VEC=10.25 to around 11.4 GPa at VEC=11.75. The trend of $E$ follows a comparable downward pattern to $H$, as $E$ decreases from an average of approximately 524.1 GPa at VEC=10.25 to around 343.8 GPa at VEC=11.75.

Based on the above analysis, the variations of several key elastic parameters of HEBs with VEC have been investigated. Although these properties have a clear overall trend driven by VEC, the key elastic parameters with the same VEC are always widely dispersed. Despite having the same VEC, HEBs formed by different elemental combinations have quite distinct mechanical characteristics. This suggests that the observed substantial fluctuations reflect a fundamental and universal pattern. Specifically, describing the changes in elastic properties in terms of the VEC alone would not take into account the significant influence of other essential factors. At a fundamental level, a significant aspect absent from the VEC description is the charge distribution within HEBs, which can differ significantly even with the same overall VEC. In order to accurately classify HEB systems, it is necessary to study and comprehend the primary mechanisms underlying the dominant elastic properties and to identify a reliable descriptor. The relative electronegativity of the constituent elements is an important factor in determining the characteristics of internal charge distribution among the atoms within a HEB structure. Therefore, the REN has the potential to serve as the primary indicator for predicting the trend of the related properties.

### 3.3 VEC−REN descriptor for precise sorting HEB

Subsequently, we used the electronegativity combined with the VEC as a new indicator to accurately describe and predict the mechanical properties of HEBs. To achieve this, we examined the 18 HEBs with the same VEC but different REN values. Specifically, three TM atoms were fixed within the same group, while the remaining TM atom passed through a series of TM atoms in an adjacent group. The key mechanical characteristics of a range of TiZrHf−(TM)B8 and VNbTa−(TM)B8 HEBs are illustrated in Figs. 8(a−c) and 8(d−f), respectively. In the TiZrHf−(TM)B8 systems, TiZrHfTaB8, TiZrHfNbB8, and TiZrHfVB8 all share the same VEC of 10.25, as shown in Fig. 8(a).

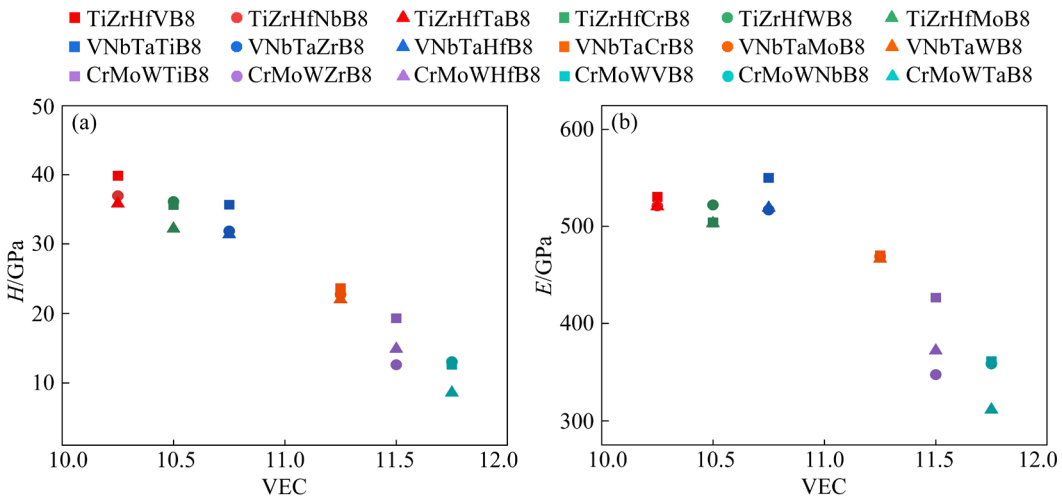


**Fig. 7** (a) Calculated hardness ($H$) as function of VEC for all diborides; (b) Calculated Young's modulus ($E$) as function of VEC for all diborides

The systematic adjustment of REN for TiZrHfTaB8, TiZrHfNbB8, and TiZrHfVB8 is achieved by the doped atoms progressing through the group VB series of Ta, Nb, and V (with REN values increasing from 1.5 to 1.6 and to 1.63, respectively), as indicated by the arrow in Fig. 8(a). Pugh's ratio, shear modulus and hardness show a monotonic rising trend as the group-VB doped TM atoms change from Ta to Nb and to V. However, these values exhibit a mostly universal decrease trend as the REN of TM atoms rises from Cr to Mo and W (the REN values increase from 1.66 to 2.16 and 2.36) in TiZrHf−(TM)B8 systems.

We further examined the VNbTa−(TM)B8 systems, where the physical characteristics are adjusted by the electronegativity of altering group-IVB and group-VIB TM atoms. The Pugh's ratio, shear modulus and hardness exhibit a rising trend as the REN of group-IVB doped TM atom increases from Hf to Zr and Ti (the REN values also increase from 1.3 to 1.33 and 1.54). This trend is comparable to the group−IVB (Ta, Nb, V) in TiZrHf−(TM)B8 systems. Physical characteristics demonstrate a decreasing trend as the REN of group-IVB doped TM elements increases from Ta (1.5) to Nb (1.6) and V (1.63), resembling the behavior observed in group-IVB (Ta, Nb, V) within TiZrHf−(TM)B8 systems.

Figure 9 plots the relationships between mechanical properties and REN for the CrMoW−(TM)B8 systems. As the REN of the doped atom increases, the CrMoW−(TM)B8 HEBs exhibit a

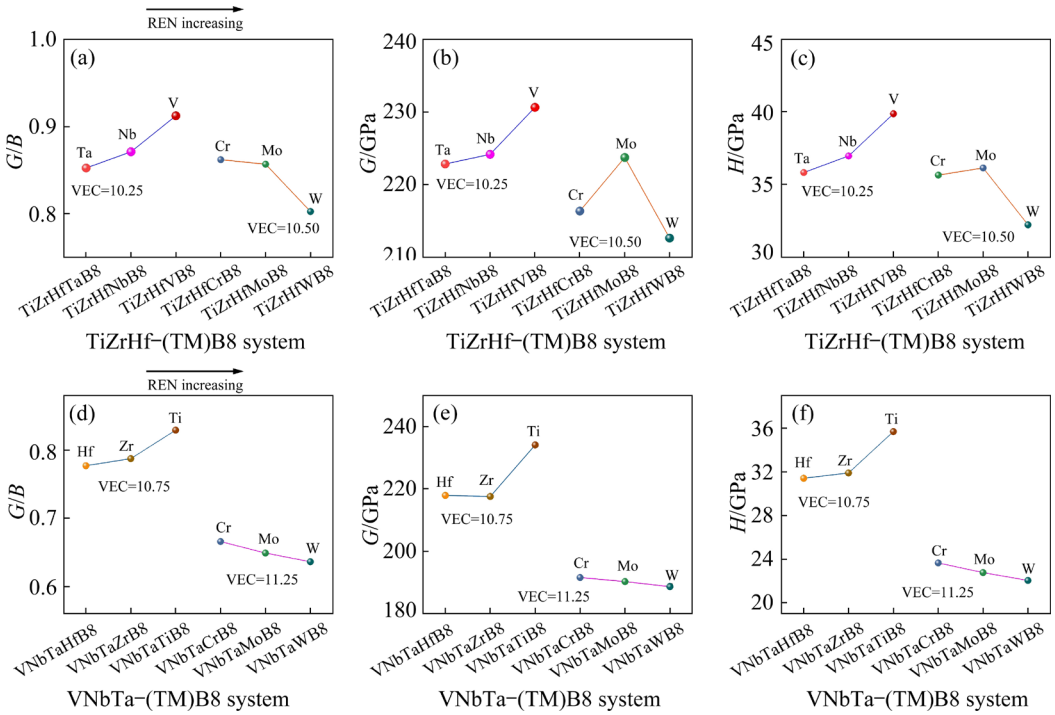


**Fig. 8** Variations of (a) Pugh's ratio ($G/B$), (b) shear modulus ($G$), and (c) hardness ($H$) for TiZrHf−(TM)B8 systems; Variations of (d) $G/B$, (e) $G$, and (f) $H$ for VNbTa−(TM)B8 systems

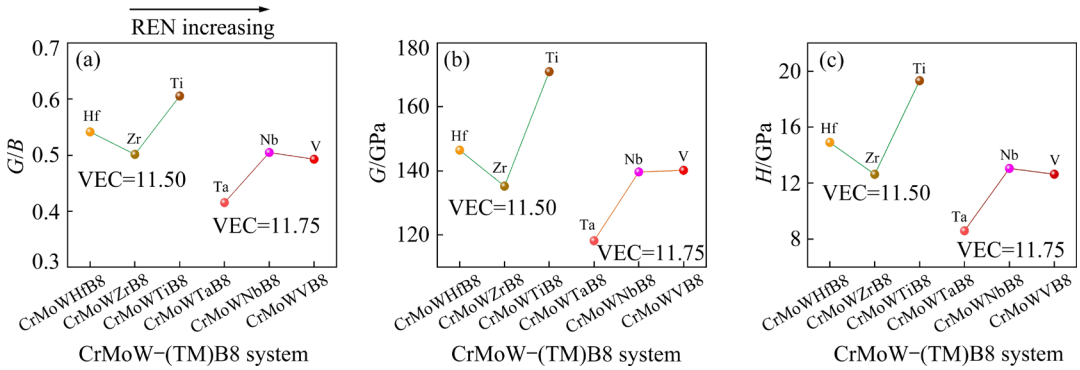


**Fig. 9** Variations of (a) Pugh's ratio ($G/B$), (b) shear modulus ($G$), and (c) hardness ($H$) for CrMoW−(TM)B8 system

predominantly monotonic decrease in the $G/B$, $G$, and $H$ values. It is worth noting that the changing trend in all major mechanical properties caused by the introduction of group-VIB (Cr, Mo, W) host atoms is opposite to that of the group-IVB or VB. Mo and W not only possess significantly higher electronegativity values compared to other TM atoms, but their electronegativity is also higher than that of B substantially. Hence, the REN of Mo and W plays a crucial role in determining the mechanical characteristics and governing the patterns.

## 4 Discussion

The electronegativity is a fundamental physical parameter that characterizes the capacity of an element to gain or donate electrons, thus determining the mechanical properties [50]. Specifically, a higher electronegativity value indicates a greater ability of an atom to attract electrons, while a lower electronegativity value indicates a stronger propensity for the atom to donate electrons. In the case of TiZrHfTaB8, TiZrHfNbB8 and TiZrHfVB8, for example, all share the same VEC of 10.25. However, the value of the REN is systematically adjusted as the doped TM atoms pass through the V, Nb, and Ta in the group VB series. The substitution of TM atoms with high electronegativity can increase charge attraction from the adjacent boron sites and boron—boron bonding regions, leading to a notable accumulation of charge around the substitution site. This apparent charge transfer forms a stronger network of B bonds and enhanced B—Nb bond binding. ZHOU et al [20] demonstrated that the enhanced covalent TM d—B p ($sp^2$) bonding has a positive effect on shear resistance, while the excessive occupation of TM dd bonding has a negative effect on shear modulus in transition metal diboride. Similar phenomena have been observed in binary and ternary carbides [51,52], in which the enhanced transition metal dd bonding has a negative effect on shear resistance. XU et al [48] discussed that the variation of bulk modulus in $TMB_2$ compounds is mainly influenced by both covalent B p—TM d interaction and TM dd bonding. The enhanced B p—TM d and TM dd bonding is beneficial to the bulk modulus $B$. Therefore, as the electronegativity of doped atoms increases from Ta to Nb and V, all the elastic parameters, shear modulus, $G/B$, and $H$ values exhibit a nearly ascending pattern.

However, in the case of VNbTaCrB8, VNbTaMoB, and VNbTaWB8 systems, where REN undergoes systematic modification as doped TM atoms pass through the VIB group series from Cr to W, the result is completely different. The key factor here is that the REN values of the doped TM atoms (Mo: 2.16 and W: 2.36) surpass not only the original TM atom Cr (1.66) value, but more significantly, also exceed that of B (2.04). This enables these doped atoms to effectively transport charge away from the B—B bonding regions. The charge transfer can weaken the strength of the B bonding network, and then the extensive weakening of covalent bonds can eventually lead to the deterioration of mechanical properties. The results of these systems demonstrate that VEC-REN can be used as a reliable descriptor to accurately classify and predict the mechanical properties of high-entropy diborides. HEBs that possess identical VECs can exhibit significantly varied characteristics as a result of the fundamentally distinct charge redistribution caused by REN.

## 5 Conclusions

(1) 18 quaternary HEBs consisting of boron and IVB, VB and VIB transition metals were systematically investigated using first-principles calculations. These HEBs are found to be thermodynamically stable, satisfying the criterion for forming single-phase solid solution structure.

(2) The relative electronegativity of the constituent transition metals is identified as a decisive indicator in regulating the widely dispersed property trends in HEBs under the VEC description. When the REN of the doped metal atoms is lower than that of boron, an increase in REN leads to higher hardness and brittleness. Conversely, when the REN of the doped metals exceeds that of boron, the HEBs exhibit softer and more ductile characteristics with increasing REN.

(3) An accurate and efficient VEC-REN descriptor is established to sort and predict mechanical properties. This work provides significant insights for discovering and predicting the HEBs and also paves the way for the rapid exploration of novel high-entropy ceramic materials with hardness-toughness balance.

## CRediT authorship contribution statement

**Yong FAN:** Investigation, Methodology, Writing − Original draft, Writing − Review & editing; **Jin-feng NIE:** Investigation, Conceptualization, Funding acquisition, Supervision, Writing − Review & editing; **Jin WANG:** Investigation, Data analysis; **Zhi-gang DING:** Methodology, Data analysis; **Wei LIU:** Supervision, Writing − Review & editing; **Yong-hao ZHAO:** Supervision, Writing − Review & editing.

## Declaration of competing interest

The authors declare that they have no known competing financial interests or personal relationships that could have appeared to influence the work reported in this paper.

## Acknowledgments

The authors are grateful to the National Natural Science Foundation of China (Nos. 52071179, 52271033), the Key Program of National Natural Science Foundation of China (No. 51931003), the Natural Science Foundation of Jiangsu Province, China (No. BK20221493), the Jiangsu Province Leading Edge Technology Basic Research Major Project, China (No. BK20222014), and the Foundation of "Qinglan Project" for Colleges and Universities in Jiangsu Province, China. We also want to thank "Changchun Computing Center" and "Eco-Innovation Center" for providing inclusive computing power and technical support of MindSpore during the completion of this paper.

## References

[1] CANTOR B, CHANG I T H, KNIGHT P, VINCENT A J B. Microstructural development in equiatomic multicomponent alloys [J]. Materials Science and Engineering A, 2004, 375/356/377: 213−218.

[2] WANG Shen, LI Da, XIONG Jun. Prediction of elastic properties of face-centered cubic high-entropy alloys by machine learning [J]. Transactions of Nonferrous Metals Society of China, 2023, 33: 518−530.

[3] TIAN Yu-sheng, ZHOU Wen-zhe, TAN Qing-biao, WU Ming-xu, QIAO Shen, ZHU Guo-liang, DONG An-ping, SHU Da, SUN Bao-de. A review of refractory high-entropy alloys [J]. Transactions of Nonferrous Metals Society of China, 2022, 32: 3487−3515.

[4] HUO Wen-yi, WANG Shi-qi, DOMINGUEZ-GUTIERREZ F J, REN Kai, KURPASKA Ł, FANG Feng, PAPANIKOLAOU S, KIM H S, JIANG Jian-qing. High-entropy materials for electrocatalytic applications: A review of first principles modeling and simulations [J]. Materials Research Letters, 2023, 11: 713−732.

[5] GUO Lin, GU Ji, DAI Yi-long, LIN Jian-guo, SONG Min. Heterogeneous microstructure and mechanical properties of carbon-doped FeCoCrNiMn high-entropy alloy [J]. Transactions of Nonferrous Metals Society of China, 2024, 32: 1893−1970.

[6] OSMAN H, LIU Lin. Additive manufacturing of high-entropy alloy composites: A review [J]. Transactions of Nonferrous Metals Society of China, 2023, 33: 1−24.

[7] CHEN Yu-yao, NIE Jin-feng, FAN Yong, GU Lei, XIE Ke-wei, LIU Xiang-fa, ZHAO Yong-hao. Enhancing strength–ductility synergy of $AlN_p$/Al composite by regulating heterostructure of matrix grain and particle distribution [J]. Transactions of Nonferrous Metals Society of China, 2024, 34: 1049−1064.

[8] WANG Xin, CORTEZ J, DUPUY A D, SCHOENUNG J M, BOWMAN W J. High entropy oxide (Co,Cu,Mg,Ni,Zn)O exhibits grain size dependent room temperature deformation [J]. Materials Research Letters, 2022, 11: 196−204.

[9] NIE Jin-feng, ZHI Ya-ting, FAN Yong, ZHAO Yong-hao, LIU Xiang-fa. One-step synthesis of high-entropy diborides with hierarchy structure and high hardness via aluminum-melt reaction method [J]. Materials Research Letters, 2023, 12: 88−96.

[10] MA Meng-dong, YE Bei-lin, HAN Yang-jie, SUN Lei, HE Ju-long, CHU Yan-hui. High-pressure sintering of ultrafine-grained high-entropy diboride ceramics [J]. Journal of the American Ceramic Society, 2020, 103: 6655−6658.

[11] WEN Zi-hao, TANG Zhong-yu, LIU Yi-wen, ZHUANG Lei, YU Hu-lei, CHU Yan-hui. Ultrastrong and high thermal insulating porous high-entropy ceramics up to 2000 °C [J]. Advanced Materials, 2024, 36: 2311870.

[12] YE Bei-lin, WEN Tong-qi, MANH C N, HAO Lu-yao, WANG Cai-zhuang, CHU Yan-hui. First-principles study, fabrication and characterization of $(Zr_{0.25}Nb_{0.25}Ti_{0.25}V_{0.25})C$ high-entropy ceramics [J]. Acta Materialia, 2019, 170: 15−23.

[13] MA Meng-dong, SUN Ya-nan, WU Ying-ju, ZHAO Zhi-sheng, YE Li, CHU Yan-hui. Nanocrystalline high-entropy carbide ceramics with improved mechanical properties [J]. Journal of the American Ceramic Society, 2022, 105: 606−613.

[14] NAYAK G K, KRETSCHMER A, MAYRHOFER P H, HOLEC D. On correlations between local chemistry, distortions and kinetics in high entropy nitrides: An ab initio study [J]. Acta Materialia, 2023, 255: 118951.

[15] TANG Zhong-yu, WEN Zi-hao, LIU Yi-wen, ZHUANG Lei, YU Hu-lei, CHU Yan-hui. Rapid experimental screening of high-entropy diborides for superior oxidation resistance [J]. Advanced Functional Materials, 2024, 34: 2312239.

[16] WEN Zi-hao, TANG Zhong-yu, MENG Hong, ZHUANG Lei, YU Hu-lei, CHU Yan-hui. Ultrafast synthesis of high-entropy carbides up to 3273 K for superior oxidation resistance [J]. Cell Reports Physical Science, 2024, 5: 101821.

[17] WEN Zi-hao, MENG Hong, JIANG Sheng-da, TANG Zhong-yu, LIU Yi-wen, CHU Yan-hui. Non-equimolar $(Hf,Zr,Ta,W)B_2$ high-entropy diborides enable superior oxidation resistance [J]. Science China Materials, 2023, 66: 3213−3222.

[18] ZHANG Pan, LIU Xiong-jun, CAI An-hui, DU Qing, YUAN Xiao-yuan, WANG Hui, WU Yuan, JIANG Sui-he, LU Zhao-ping. High-entropy carbide-nitrides with enhanced toughness and sinterability [J]. Science China Materials, 2021, 64: 2037−2044.

[19] ZHANG Yan, SUN Shi-Kuan, ZHANG Wei, YOU Yang, GUO Wei-ming, CHEN Zhi-wei, YUAN Jin-hao, LIN Hua-tay. Improved densification and hardness of high-entropy diboride ceramics from fine powders synthesized via borothermal reduction process [J]. Ceramics International, 2020, 46: 14299−14303.

[20] ZHOU Yan-chun, XIANG Hui-min, FENG Zhi-hai, LI Zhong-ping. General trends in electronic structure, stability, chemical bonding and mechanical properties of ultrahigh temperature ceramics $TMB_2$ (TM = transition metal) [J]. Journal of Materials Science & Technology, 2015, 31: 285−294.

[21] QIN Ming-de, GILD J, WANG Hao-ren, HARRINGTON T, VECCHIO K S, LUO Jian. Dissolving and stabilizing soft $WB_2$ and $MoB_2$ phases into high-entropy borides via boron-metals reactive sintering to attain higher hardness [J]. Journal of the European Ceramic Society, 2020, 40: 4348−4353.

[22] WANG Chun-yang, QIN Ming-de, LEI Tian-jiao, HE Yu-bin, KISSLINGER K, RUPERT Timothy J, LUO Jian, XIN H L. Synergic grain boundary segregation and precipitation in W- and W−Mo-containing high-entropy borides [J]. Journal of the European Ceramic Society, 2021, 41: 5380−5387.

[23] WEN Tong-qi, YE Bei-lin, LIU Hong-hua, NING Shan-shan, WANG Cai-zhuang, CHU Yan-hui. Formation criterion for binary metal diboride solid solutions established through combinatorial methods [J]. Journal of the American Ceramic Society, 2020, 103: 3338−3348.

[24] JIANG Shan, SHAO Lin, FAN Tou-wen, DUAN Jia-ming, CHEN Xiao-Tao, TANG Bi-Yu. Elastic and thermodynamic properties of high entropy carbide (HfTaZrTi)C and (HfTaZrNb)C from ab initio investigation [J]. Ceramics International, 2020, 46: 15104−15112.

[25] WANG Ya-ping, GAN Guo-pong, WANG Wei, YANG Yan, TANG Bi-yu. Ab initio prediction of mechanical and electronic properties of ultrahigh temperature high-entropy ceramics $(Hf_{0.2}Zr_{0.2}Ta_{0.2}M_{0.2}Ti_{0.2})B_2$ (M=Nb, Mo, Cr) [J]. Physica Status Solidi B−Basic Solid State Physics, 2018, 255: 1800011.

[26] GUO Sheng, LIU C T. Phase stability in high entropy alloys: Formation of solid-solution phase or amorphous phase [J]. Progress in Natural Science: Materials International, 2011, 21: 433−446.

[27] LIU Shi-yu, LIU Chang-ming, ZHANG Shuo-xin, LIU Shi-yang, LI De-jun, LI Ya-ping, WANG San-wu. Phase diagram and mechanical properties of fifteen quaternary high-entropy metal diborides: First-principles calculations and thermodynamics [J]. Journal of Applied Physics, 2022, 131: 075105.

[28] GU Xin-lei, LIU Chang, GUO Hao, ZHANG Kan, CHEN Chang-feng. Sorting transition-metal diborides: New descriptor for mechanical properties [J]. Acta Materialia, 2021, 207: 116685.

[29] KIM J. Applicability of special quasi-random structure models in thermodynamic calculations using semi-empirical Debye–Grüneisen theory [J]. Journal of Alloys and Compounds, 2015, 650: 564−571.

[30] WALLE A V D. Multicomponent multisublattice alloys, nonconfigurational entropy and other additions to the Alloy Theoretic Automated Toolkit [J]. Calphad, 2009, 33: 266−278.

[31] PERDEW, J P, BURKE K, ERNZERHOF M. Generalized gradient approximation made simple [J]. Physical Review Letters, 1997, 77: 3865.

[32] BLÖCHL P E. Projector augmented-wave method [J]. Physical Review B, 1994, 50: 17953−17979.

[33] LI Ke-yan, XUE Dong-feng. Estimation of electronegativity values of elements in different valence states [J]. Journal of Physical Chemistry A, 2006, 110: 11332−11337.

[34] HILL R. The elastic behavior of crystalline aggregate [J]. Proceedings of Physical Society: Section A, 1952, 65: 349−354.

[35] WANG Xin, ZHANG Yu-ting, LIU Peng-chuang, YAN Jia-wei, MO Wen-lin, ZHANG Peng-cheng, CHEN Xing-qiu. Ductile-to-brittle transition and materials' resistance to amorphization by irradiation damage [J]. RSC Advances, 2016, 6: 44561−44568.

[36] THOMPSON R P, CLEGG W J. Predicting whether a material is ductile or brittle [J]. Current Opinion in Solid State and Materials Science, 2018, 22: 100−108.

[37] TIAN Yong-jun, XU Bo, ZHAO Zhi-sheng. Microscopic theory of hardness and design of novel superhard crystals [J]. International Journal of Refractory Metals and Hard Materials, 2012, 33: 93−106.

[38] FELTRIN A C, HEDMAN D, AKHTAR F. Transformation of metastable dual-phase $(Ti_{0.25}V_{0.25}Zr_{0.25}Hf_{0.25})B_2$ to stable high-entropy single-phase boride by thermal annealing [J]. Applied Physics Letters, 2021, 119: 161905.

[39] FENG Lun, FAHRENHOLTZ W, HILMAS G E, MONTEVERDE F. Effect of Nb content on the phase composition, densification, microstructure, and mechanical properties of high-entropy boride ceramics [J]. Journal of the European Ceramic Society, 2021, 41: 92−100.

[40] FAILLA S, GALIZIA P, FU Shuai, GRASSO S, SCITI D. Formation of high entropy metal diborides using arc-melting and combinatorial approach to study quinary and quaternary solid solutions [J]. Journal of the European Ceramic Society, 2020, 40: 588−593.

[41] LIU Shi-Yu, ZHANG Shuo-xin, LIU Shi-yang, LI De-Jun, NIU Zhi-qiang, LI Ya-ping, WANG San-wu. Stability and mechanical properties of single-phase quinary high-entropy metal carbides: First-principles theory and thermodynamics [J]. Journal of the European Ceramic Society, 2022, 42: 3089−3098.

[42] TSAI Ming-Hung, YEH Jien-Wei. High-entropy alloys: A critical review [J]. Materials Research Letters, 2014, 2: 107−123.

[43] YE Bei-lin, WEN Tong-qi, HUANG Ke-han, WANG Cai-zhuang, CHU Yan-hui. First-principles study, fabrication, and characterization of $(Hf_{0.2}Zr_{0.2}Ta_{0.2}Nb_{0.2}Ti_{0.2})C$ high-entropy ceramic [J]. Journal of the American Ceramic Society, 2019, 102: 4344−4352.

[44] HAO Xian-feng, XU Yuan-hui, WU Zhi-jian, ZHOU De-feng, LIU Xiao-juan, CAO Xue-qiang, MENG Jian. Low-compressibility and hard materials $ReB_2$ and $WB_2$: Prediction from first-principles study [J]. Physical Review B, 2006, 74: 224112.
[45] CHERNIKOV M A, OTT H R, BIANCHI A, MIGLIORI A, DARLING T W. Elastic moduli of a single quasicrystal of decagonal Al−Ni−Co: Evidence for transverse elastic isotropy [J]. Physical Review Letters, 1998, 80: 321−324.
[46] PUGH S F. XCII. Relations between the elastic moduli and the plastic properties of polycrystalline pure metals [J]. Philosophical Magazine, 1954, 45: 823−843.
[47] SHEIN I R, IVANOVSKII A L. Elastic properties of mono-and polycrystalline hexagonal $AlB_2$-like diborides of s, p and d metals from first-principles calculations [J]. Journal of Physics: Condensed Matter, 2008, 20: 415218.
[48] XU Xue-wen, FU Kun, YU Man, LU Zun-ming, ZHANG Xing-hua, LIU Guo-dong, TANG Cheng-chun. The thermodynamic, electronic and elastic properties of the early-transition-metal diborides with $AlB_2$-type structure: A density functional theory study [J]. Journal of Alloys and Compounds, 2014, 607: 198−206.
[49] TSE J S. Intrinsic hardness of crystalline solids [J]. Journal of Superhard Materials, 2010, 32: 177−191.
[50] ZHANG Hong-tao, FU Hua-dong, HE Xing-qun, WANG Chang-sheng, JIANG Lei, CHEN Long-qing, XIE Jian-xin. Dramatically enhanced combination of ultimate tensile strength and electric conductivity of alloys via machine learning screening [J]. Acta Materialia, 2020, 200: 803−810.
[51] WANG Jing-yang, ZHOU Yan-chun. Dependence of elastic stiffness on electronic band structure of nanolaminate $M_2AlC$(M=Ti,V,Nb, and Cr) ceramics [J]. Physical Review B, 2004, 69: 214111.
[52] WANG Jing-yang, ZHOU Yan-chun. Ab initio elastic stiffness of nano-laminate $(M_xM'_{2-x})AlC$ (M and M′=Ti, V and Cr) solid solution [J]. Journal of Physics−Condensed Matter, 2004, 16: 2819−2827.

# 用于筛选高熵二硼化物力学性能的复合描述符

范 勇[1]，聂金凤[1]，王 进[1]，丁志刚[1]，刘 伟[1,2]，赵永好[1,3]

1. 南京理工大学 材料科学与工程学院 纳米异构材料中心，南京 210094；
2. 中国科学院 长春应用化学研究所 稀土资源利用国家重点实验室，长春 130022；
3. 河海大学 材料科学与工程学院，常州 213022

**摘 要**：采用第一性原理计算研究了由 IVB、VB、VIB 过渡金属(TM)和硼元素组成的 18 种四元高熵二硼化物(HEBs)组成成分与性能的关系。通过建立价电子浓度−相对电负性(VEC−REN)复合描述符有效预测 HEBs 的力学性能。结果表明，在 VEC 固定的情况下，如果掺杂 TM 原子的 REN 小于硼原子的 REN 时，TM 原子 REN 的增加会导致 HEBs 变得更硬更脆；然而，当掺杂 TM 原子的 REN 超过硼原子的 REN 时，随着 TM 原子 REN 的增加，HEBs 变得更软更韧。利用 VEC−REN 复合描述符可以准确分类和预测不同成分 HEBs 的力学性能，为新型高熵陶瓷材料的快速设计开发提供重要的理论指导。

**关键词**：第一性原理；高熵二硼化物；价电子浓度；相对电负性；力学性能

**(Edited by Bing YANG)**